


First principles study on the electronic structure properties of Keggin polyoxometalates on Carbon substrates for solid-state devices

Jesús Muñiz^{1,2}  · Christian Celaya³ · Ana Mejía-Ozuna⁴ · Ana Karina Cuentas-Gallegos¹ · L. M. Mejía-Mendoza¹ · Miguel Robles¹ · Maximiliano Valdéz¹

Received: 18 October 2016 / Accepted: 4 January 2017 / Published online: 12 January 2017
© Springer-Verlag Berlin Heidelberg 2017

Abstract Carbon has shown to give excellent performance in electrodes of energy storage devices, such as Li-ion batteries and supercapacitors. The grafting of polyoxometalates (POM) at carbon has scarcely been explored at the theoretical and experimental level, and the mechanism behind the chemical bonding between POM and carbon has not been fully understood. In order to give insights into these issues, an electronic structure study was carried out on the following POM systems adsorbed on carbon: PdMo₁₂, RuNb₁₂, SiMo₁₂, PMo₁₂ and SiW₁₂. The prediction of the existence and chemical stability of PdMo₁₂ and RuNb₁₂ systems is reported for the first time. All systems were fully optimized with the nominal charges and also neutralized with counterions, as a benchmark to elucidate an optimal scheme that models the interaction in these nanocomposite systems. The POM/carbon attraction lies at about 250 pm in

average, which may be addressed to a non-covalent bonding of the electrostatic-type, where the van der Waals contribution may also play a role. The density of states is evidently increased around the Fermi level in all POM/carbon systems. This may be due to the rising of new trajectories that ions may follow at the electrode of a solid-state device, such as a supercapacitor, giving as a result the strengthening of density current values and pseudocapacitive properties than those observed in pristine carbon systems. It was found that the SiWO₁₂ and RuNb₁₂ POM systems may be more feasible to be adsorbed on carbon substrates and may not require functional groups to allow POM retention. These systems represent potential candidates to be considered in nanohybrid electrodes for solid-state applications.

Keywords Density functional theory · Energy storage · Polioxometalates · Solid-state devices · Electrostatic-type interactions

Electronic supplementary material The online version of this article (doi:10.1007/s00214-017-2049-3) contains supplementary material, which is available to authorized users.

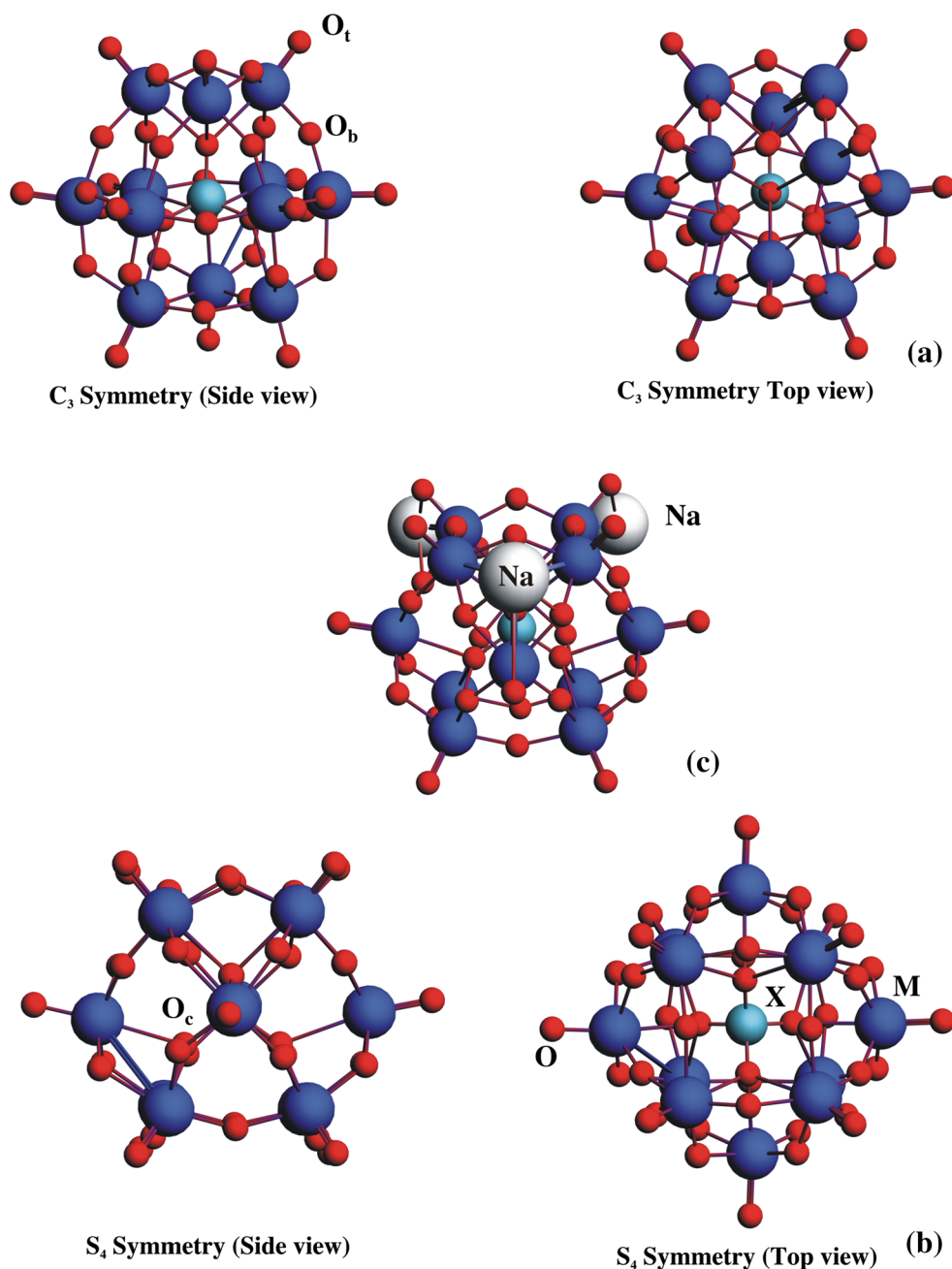
✉ Jesús Muñiz
jms@ier.unam.mx

- ¹ Instituto de Energías Renovables, Universidad Nacional Autónoma de México, Priv. Xochicalco s/n, Col. Centro, 62580 Temixco, Morelos, Mexico
- ² CONACYT-Universidad Nacional Autónoma de México, Priv. Xochicalco s/n, Col. Centro, 62580 Temixco, Morelos, Mexico
- ³ Departamento de Baja Dimensionalidad, Instituto de Investigaciones en Materiales, Universidad Nacional Autónoma de México, Apartado Postal 70-360, Ciudad de México, Mexico
- ⁴ Programa Académico de Ingeniería en Energía, Universidad Politécnica de Chiapas, Carretera Tuxtla-Villaflores km 1+500, 29150 Suchiapa, Chiapas, Mexico

1 Introduction

The quest of energy storage and conversion materials has become a priority area of research in material science due to the need of efficient storage of energy coming for instance, from wind or solar devices [1, 2]. The development of molecular batteries and supercapacitors, where carbon-based electrodes are the leading materials, has triggered remarkable breakthroughs [3, 4]. This is the case in the incorporation of the chemistry of metallic oxides, known as polyoxometalates (POM) of the Keggin-type onto carbon matrices, such as graphene [5–7], single-walled carbon nanotubes (SWCNT) [3, 4] and the nanoporous carbon known as VulcanTM [8]. The generic formulation of the cage-like Keggin POM structures is $[XM_{12}O_{40}]^{n-}$ where X

Fig. 1 **a** C_3 and **b** S_4 orientations of the system $XM_{12}O_{40}^{n-}$, with $X = Pd, P, Ru, Si$ and $M = Mo, Nb, W$ and $n = 2, 3, 4, 8$. O_t , O_b and O_c are an oxygen atom at the *top*, at a bridging bond and at the central peripheral of the POM system, respectively. **c** A perspective of the n Na-counterions introduced in the POM system to neutralize the overall charge. *Note* that n may take the values $n = 2, 3, 4$ and 8 . C_3 and S_4 orientations are with respect to an axis crossing the center of the POM. Such axis is perpendicular with respect to the plane of a graphene sheet



corresponds to a nonmetal (see Fig. 1), such as P and M is a metal such as Mo, W or V [9]. For simplicity, we can also use the term XM_{12} to denote a $[XM_{12}O_{40}]^{n-}$ system. The applicability regarding the physical and chemical properties of POMs is ample, since they have been used as amperometric sensors [10, 11], water-splitting systems [12], fuel cells [13] and electrochemical sensors of glucose [14] and they have widely been spread as electrode materials in Li-ion batteries [15, 16] and supercapacitors [3, 4, 17–19]. Specifically, the last two applications require the attachment of POMs to a conductive substrate to take advantage of their electronic conductivity properties, such as carbon

materials. This is the reason why the POM anchoring on carbon substrates is highly desirable to achieve enhanced charge retention and also to avoid dissolution. POMs present the ability to be adsorbed on a variety of carbon substrates as graphene [5, 6], carbon nanotubes [4, 18, 20], aerogels [19] or activated carbons [21, 22]. This has highly improved fast lithium-ion diffusion when compared to pristine carbon substrates, [15, 16] as implemented in Li-ion batteries. Furthermore, POM/nanohybrid materials are considered to be a competing alternative to the use of RuO_2 pseudocapacitive material in supercapacitor electrode applications. Experimentally, POMs have been

attached to carbon substrates through their redox activity. For instance, the system $\text{PMo}_{12}\text{O}_{40}^{3-}$ (or readily PMo_{12}) has been anchored to carbon [20, 21], which has been evidenced by the color shifting from yellow solution to a blue solution, indicating a reduction of POM in the redox process [23]. In a recent study [8], our group also found that functional groups may be incorporated to an amorphous carbon substrate (namely VulcanTM carbon) in a grafting process by using diazonium salts. The POM clusters were grafted onto the amorphous carbon matrix via a $\varphi\text{-OH}$ and $\varphi\text{-NH}_2$ functional groups, and also in the absence of both. It was found that the presence of POM clusters increases the density current from that found on pristine VulcanTM carbon, and the density current is significantly enhanced after the deposition of PMo_{12} cluster onto VulcanTM carbon functionalized with $\varphi\text{-OH}$ and $\varphi\text{-NH}_2$. Particularly, a maximum in density current found at the voltammograms is reached with the $\varphi\text{-OH}$ functional group. Tessonnier et al. [7] synthesized the group of POMs $\text{H}_3\text{PM}_{12}\text{O}_{40}$, $\text{H}_3\text{PW}_{12}\text{O}_{40}$ and $\text{H}_4\text{PMO}_{11}\text{VO}_{40}$ supported on oxygen and alkyl-functionalized graphene sheets, and they found that these materials give the ability to disperse POMs in environments where they would not dissolve if unsupported. As another example, the POM $\text{H}_3\text{PW}_{12}\text{O}_{40}$ was co-assembled [24] onto graphene oxide nanosheets using layer-by-layer deposition. This nanohybrid system was addressed as photomasks to produce conductive patterns of reduced graphene oxide, and it was used as an efficient microelectrode for photodetector devices. On the other hand, Xu et al. [25] explored the system $\text{SiW}_{11}\text{VO}_{40}$ deposited on graphene, by introducing it into a TiO_2 film as a photovoltaic material. They found a significant photocurrent response, attributable to the photoinduced electrons of $\text{SiW}_{11}\text{VO}_{40}$, resulting in a potential material with a lower energy level than that of the conduction band of TiO_2 . Wang et al. [5] prepared a $\text{H}_4\text{SiW}_{12}\text{O}_{40}$ POM system supported on reduced graphene oxide nanosheets. It was found that the nanocomposite presents an increased capacity of 275 mAhg^{-1} as cathode active material for Li storage. This is almost two times larger than the capacity found in pure SiW_{12} .

The nature of bonding between the carbon substrates and the POM systems has been a subject of debate [4], and it has been elucidated in a reduced group of works performed with *ab initio* methodologies and molecular dynamics. For instance, Wen et al. [26] reported a DFT study on the interaction of SWCNT and the PMo_{12} cluster via a tetrabutylammonium (TBA) linker. From a density of states analysis performed at the lowest energy configurations, it was found that the semiconducting character of the SWCNT is changed to a metallic character instead, after the anchoring of the PMo_{12} system onto the SWCNT surface. This may

be suitable if implemented on molecular batteries or supercapacitors. An experimental/theoretical (DFT) work was performed by Yang et al. [27] on a supercapacitor made of a graphene substrate, which was functionalized with PMo_{12} clusters and a polymeric ionic liquid (PIL), acting as an interfacial linker. It was found that the presence of the PIL increases redox reactions of PMo_{12} , stimulating an improved charged transfer that enhances the capacitance in the supercapacitor system. On the other hand, by a DFT study [28], it was found that if POMs are immersed into a solvent, the POM consumes hydroxyl groups, producing water and a covalent bonding with cristobalite surfaces. A combined DFT/MD study performed by Aparicio [29] revealed an adsorption of the SiW_{12} system onto a Ag surface, where the solvent was responsible for the reduction of POMs. Finally, a DFT study was recently performed by our group [30] on the PMo_{12} systems grafted on graphene. It was found that a non-covalent/electrostatic bonding at PMo_{12} /graphene interface rules the attraction. It was also found that the presence of $\varphi\text{-NH}_2$ and $\varphi\text{-OH}$ functional groups stimulates a covalent attraction with PMo_{12} . This was addressed to the empirical observation that implies that the functional groups aid on the PMo_{12} adsorption on carbon surfaces. It was also found that POM retention originates new electronic states that ions may track in the electrochemical devices. The search of novel nanohybrid materials that involve POM retention on carbon matrices is of high relevance, since the improved electronic features coming from the interaction may be directly implemented into the development of solid-state devices. As previously stated, the exploration of POM/carbon nanohybrid systems at the theoretical level is only limited to a small group. As suggested by Genovese and Lian [3], a deeper understanding from fundamental grounds on the mechanism ruling the interactions on POM systems and carbon is of high priority for sustainable research on energy storage materials and other applications involving solid-state devices based on POM nanohybrid systems. The aim of this work is to understand the electronic structure properties that may play a role on the performance of unprecedented POM/carbon systems, with potential applications on solid-state devices such as molecular batteries and supercapacitors, via a systematic study on the series of $[\text{XM}_{12}\text{O}_{40}]^{n-}$ systems where $\text{X} = \text{P}, \text{Pd}, \text{Si}$ and Ru , and $\text{M} = \text{Mo}, \text{W}$ and Nb , n is dependant on the overall valence of the POM system. Particularly, the systems with $\text{X} = \text{Ru}$ and $\text{M} = \text{Nb}$ are unpublished POMs at the theoretical and experimental levels. Our results may give new insights into the development of materials that may be of potential interest to provide improved specific capacitances from those found in available systems.

2 Computational details

An extended model of graphene with 112 carbon atoms was considered to include periodic conditions and to simulate a network where the metallic POM clusters may interact with carbon, recreating a fragment of a typical carbon electrode from a supercapacitor or battery. In order to study the electronic structure properties of a series of nanohybrid XM_{12} /Graphene systems, full geometry optimizations were performed using density functional theory (DFT) at the generalized gradient approximation and local density approximation (GGA and LDA levels, respectively). This study was performed in order to have a wider landscape of the particularities risen by using different approaches for the same applications, and we further selected the approach that better suited the analysis on energy storage properties. From the optimized structures, we computed adsorption energies, structural parameters, density differences, charge transfer, total density of states (DOS) and projected density of states (PDOS). The DFT/GGA calculations were performed using the PBE (Perdew–Burke–Ernzerhof) level of theory, and it was also used as a functional that includes a van der Waals correction, which is important to describe London-type interactions present at the interface of the hybrid material [30]. For comparison, the calculations were also carried out at the LDA/CA level and in both cases, pseudopotentials were used for all atoms as implemented in the SIESTA ab initio package [31–33]. The computational code uses the Troullier–Martins non-local form of norm-conserving pseudopotentials and localized atomic orbitals as basis sets. The double- ζ plus polarization basis set (DZP) was used for all elements defined in the series of the title compounds. In order to neutralize the overall charge in the five series of systems, n counterions were included in the relaxation, depending on the system under study. That is, $n = 2, 3, 8, 4$ and 4 for $\text{PdMo}_{12}/\text{G}$, PMo_{12}/G , $\text{RuNb}_{12}/\text{G}$, $\text{SiMo}_{12}/\text{G}$ and SiW_{12}/G , respectively. The systems PdMo_{12} and RuNb_{12} have not been synthesized so far, and we propose a theoretical prediction from first-principle calculations. The values of the overall charges for these systems were assigned in accordance with the general rule for POM valency assignment [34, 35]. The overall charges for the PMo_{12} , SiMo_{12} and SiW_{12} were assigned from experimental data [36, 37]. The counterions were explicitly introduced by using a standardized methodology [30, 38] by adding $n\text{Na}^+$ cations. The n cations were initially located close to the oxygen atoms above the equatorial plane of the POMs, allowing the XM_{12}/G systems to be relaxed during the optimizations. The interaction with bridging oxygens around the POM system was only considered for all situations (see Fig. 1c). For the Na cations, a basis set restricted to the s -orbital was defined and a small cutoff radius of

0.497 Bohr was introduced. Furthermore, an equivalent real-space mesh cutoff of 250 Ry was also introduced as given by Kostyrko et al. [38] and Wen et al. [39]. Using this scheme, the Na atom is modeled as a point charge with unitary charge $+|e|$. In all calculations, the unit cell has the dimension $18.33 \times 18.57 \times 31.00 \text{ \AA}$, which allows the systems to be confined in a periodic lattice. Considering this cell size, the z direction presents a vacuum separation that allows to model the layer structure. It has been shown that this separation avoids spurious interactions with images in the periodic lattice for graphene and XM_{12}/G systems. A threshold of 0.01 eV \AA^{-1} was used for the final forces in all geometrical optimizations, as the convergence criteria, 10^{-5} electrons for the electron density and 10^{-5} eV for the total energy of the systems. A Monkhorst and Pack [40] grid with $3 \times 3 \times 1$ k -point for the primitive cell was implemented in order to sample the Brillouin zone. On the other hand, the electronic structure properties that may give insights into energy storage properties were analyzed. In this regard, the energetic stability of the title compounds was predicted by computing the adsorption energies (ΔE_a) in accordance with Eq. 1:

$$\Delta E_a = E_T - E_{\text{XM}_{12}} - E_G, \quad (1)$$

where E_T stands for the total energy of XM_{12}/G hybrid system with $X = \text{Pd}, \text{P}, \text{Ru}$ and Si , while $M = \text{Mo}, \text{Nb}, \text{W}$. $E_{\text{XM}_{12}}$ is the total energy of the XM_{12} isolated cluster in the same unit cell, and E_G corresponds to the total energy of the carbon substrate inside the same unit cell. The adsorption energies were also computed using a van der Waals density functional (vdW-DF) as outlined by Dion et al. [41], in order to compare with the results given by the DFT/GGA method. The latter was performed, since it is known that DFT/GGA computations are not fully reliable where the adsorption is ruled by London attractions of the van der Waals-type. As a result, only slight deviations from the GGA values were found in those calculations, indicating that the GGA/PBE approach appears to be reliable to compute this electronic structure property on this type of systems.

Charge transfer among the XM_{12} title systems and the carbon substrate was also studied in accordance to the Mulliken population analysis [42]. As it is well known, the scheme is highly sensitive to the basis set used. As a consequence, we are interested to provide qualitative trends in the electronic structure behavior of these nanohybrid ensembles. The method given by Arellano et al. [43] was implemented, where the charge density is partitioned in real space in order to state the interaction and quantitatively verify the charge transfer between the two subsystems under study, namely XM_{12} and graphene. Further, the charge transfer (ΔQ) is defined as:

$$\Delta Q = \sum Q_T - \sum Q_{XM_{12}} - \sum Q_G, \quad (2)$$

where $\sum Q_T$ represents the sum of all charges at each of the atoms in the nanohybrid system; $\sum Q_{XM_{12}}$ and $\sum Q_G$ are the total sum of the charges at the isolated POM XM_{12} system and graphene, respectively. In order to complete Arellano's scheme, the isosurfaces of the total charge density difference $\rho_{\text{diff}}(r)$ were mapped for all configurations in the title compounds. In this regard, $\rho_{\text{diff}}(r)$ was plotted in the molecular viewer VESTA [44], according to Eq. 3

$$\rho_{\text{diff}}(r) = \rho_{XM_{12}/G}(r) - \rho_{XM_{12}}(r) - \rho_G(r), \quad (3)$$

where $\rho_{XM_{12}/G}(r)$ refers to the charge density of the XM_{12} cluster adsorbed on the carbon substrate; $\rho_{XM_{12}}(r)$ is the charge density of the XM_{12} clusters in the series and $\rho_G(r)$ corresponds to the charge density of graphene, both in the same unit cell.

3 Results and discussion

3.1 Structural parameters and adsorption energies

Full geometry optimizations were performed through all title structures XM_{12}/G , with $X = \text{Pd, P, Ru}$ and Si , while $M = \text{Mo, Nb, W}$. The $\text{P}Mo_{12}$ system previously studied experimentally and theoretically by our group [8, 30] is also considered in the present work, since it may be used as a reference to the title systems unexplored at the theoretical or experimental level. In all cases, a POM interacts with a graphene sheet, considered as the simplest model of a carbon substrate in 2D. Note that such a model may also be valid in a 3D section of a nanoporous carbon, as the graphene-like structure is present on the surfaces generated using molecular dynamics as suggested by Gogotsi et al. [45] and our group [46]. Due to the high symmetry (T_d point group) found on the XM_{12} Keggin clusters, we only identified two different interacting orientations of the POM with the graphene sheet, that is, at a C_3 axis of symmetry located along the center of the POM (as it is evidenced in the top view depicted in Fig. 1a), and a S_4 axis of symmetry located along the center of the Keggin structure (see Fig. 1b). Considering both orientations with respect to the graphene plane, it was also assumed that the metallic cluster along the central axis may interact with the layer at the top of a carbon atom (T-orientation), at the center of the bridge between two C atoms (B-orientation) and exactly at the center of a hollow ring (H-orientation) on the honeycomb-like structure of graphene (see Fig. 2). Taking the latter into account, six different orientations of the XM_{12} clusters at graphene were fully relaxed, using the following notation: $C_3\text{-B}$, $C_3\text{-H}$, $C_3\text{-T}$, $S_4\text{-B}$, $S_4\text{-H}$ and $S_4\text{-T}$, corresponding to the C_3 and S_4 interacting

Table 1 Main structural parameters of the isolated $XM_{12}O_{40}^{n-}$ systems, with $X = \text{Pd, P, Ru, Si}$ and $M = \text{Mo, Nb, W}$

	Selected parameter			
	X-O	M-O _t	M-O _b	M-O _c
Bond lengths in pm (GGA)				
System (with counterions)				
$[\text{PdMo}_{12}\text{O}_{40}]^{2-}$	156.0	170.0	188.0	190.0
$[\text{PdMo}_{12}\text{O}_{40}]^{6-}$	218.7	173.2	198.5	192.1
$[\text{PMo}_{12}\text{O}_{40}]^{3-}$	156.0	173.0	195.0	202.0
$[\text{RuNb}_{12}\text{O}_{40}]^{8-}$	158.0	174.0	191.0	203.0
$[\text{SiMo}_{12}\text{O}_{40}]^{4-}$	155.0	172.0	199.0	186.0
$[\text{SiW}_{12}\text{O}_{40}]^{4-}$	154.0	168.0	183.0	190.0
System (charged)				
$[\text{PdMo}_{12}\text{O}_{40}]^{2-}$	156.0	170.0	196.0	203.0
$[\text{PMo}_{12}\text{O}_{40}]^{3-}$	166.0	171.0	196.0	195.0
$[\text{RuNb}_{12}\text{O}_{40}]^{8-}$	157.0	169.0	191.0	192.0
$[\text{SiMo}_{12}\text{O}_{40}]^{4-}$	155.0	170.0	196.0	204.0
$[\text{SiW}_{12}\text{O}_{40}]^{4-}$	165.0	171.0	195.0	193.0
Bond lengths in pm (LDA)				
System (with counterions)				
$[\text{PdMo}_{12}\text{O}_{40}]^{2-}$	195.0	171.0	192.0	200.0
$[\text{PMo}_{12}\text{O}_{40}]^{3-}$	157.0	173.0	196.0	205.0
$[\text{RuNb}_{12}\text{O}_{40}]^{8-}$	183.0	177.0	202.0	209.0
$[\text{SiMo}_{12}\text{O}_{40}]^{4-}$	168.0	174.0	192.0	202.0
$[\text{SiW}_{12}\text{O}_{40}]^{4-}$	166.0	171.0	187.0	192.0
System (charged)				
$[\text{PdMo}_{12}\text{O}_{40}]^{2-}$	202.0	172.0	209.0	208.0
$[\text{PMo}_{12}\text{O}_{40}]^{3-}$	157.0	171.0	193.0	205.0
$[\text{RuNb}_{12}\text{O}_{40}]^{8-}$	183.0	204.0	203.0	198.0
$[\text{SiMo}_{12}\text{O}_{40}]^{4-}$	168.0	174.0	197.0	191.0
$[\text{SiW}_{12}\text{O}_{40}]^{4-}$	166.0	171.0	191.0	192.0
System (experimental)				
$[\text{PdMo}_{12}\text{O}_{40}]^{2-}$	–	–	–	–
[47] $[\text{PMo}_{12}\text{O}_{40}]^{3-}$	151.0	164.0	244.0	192.0
$[\text{RuNb}_{12}\text{O}_{40}]^{8-}$	–	–	–	–
[36, 37] $[\text{SiMo}_{12}\text{O}_{40}]^{4-}$	163.0	168.0	183.0	201.9
[36, 37] $[\text{SiW}_{12}\text{O}_{40}]^{4-}$	163.0	170.0	189.0	194.0

symmetries of the Keggin structures with graphene at the bridge, hollow and top configurations, respectively. All geometry relaxations were performed with the GGA and LDA approaches for comparison and to understand the computational performance in these type of calculations. In order to have an overall view of the optimized structural parameters, it is presented in Table 1 the metal (M) to oxygen (O) bond lengths in the isolated POM systems by considering the averaged distances of oxygen atoms to the metal M at the top (O_t), center (O_c) and bridged (O_b) locations around the cluster, as depicted in Fig. 1. Note that the experimental structural parameters reported in

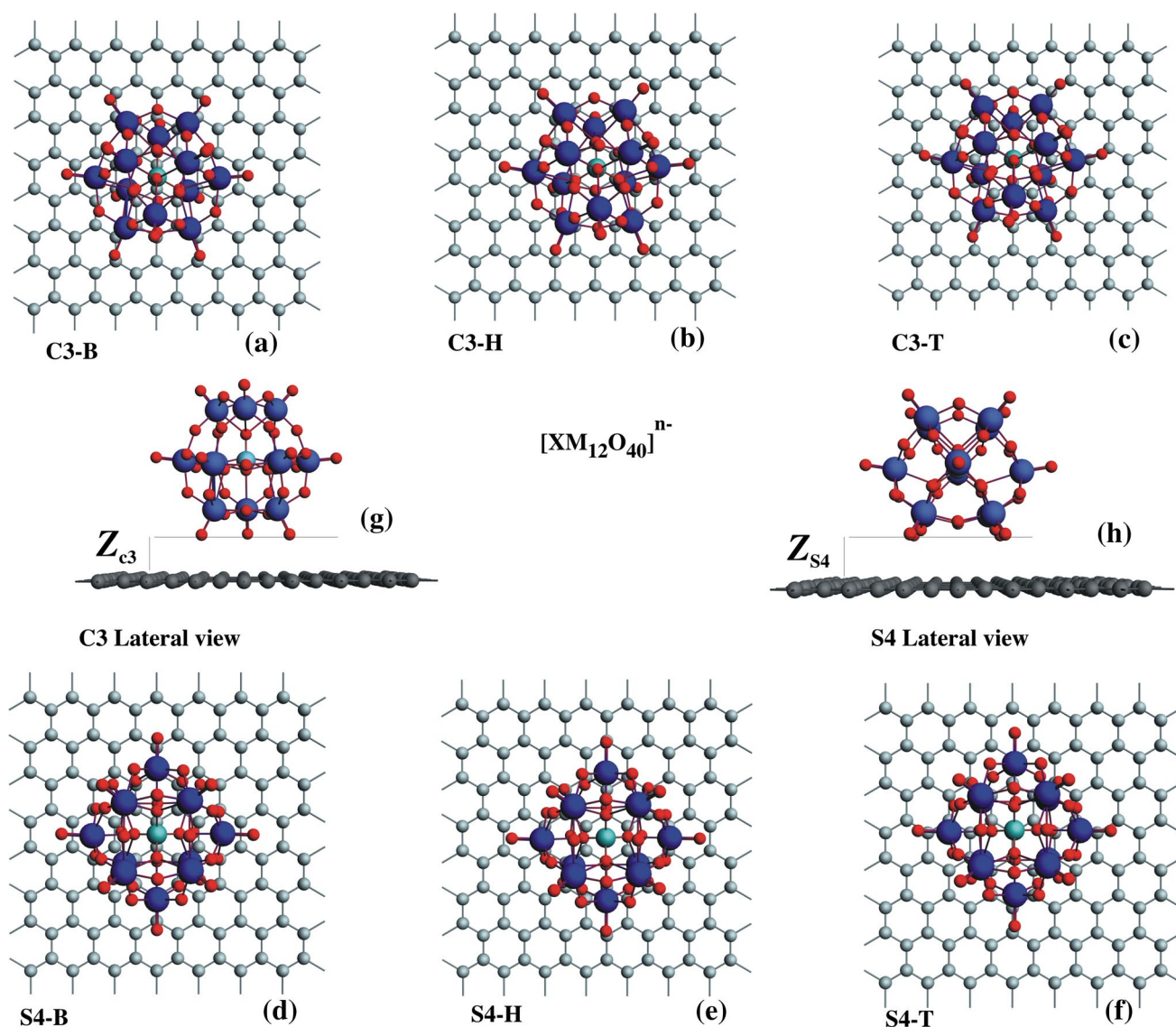


Fig. 2 Top view of the unit cell where the XM_{12} system, interacts with graphene at **a** C₃-B configuration (i.e., in bridge between 2 C atoms), **b** C₃-H configuration (i.e., at a hollow carbon ring), **c** C₃-T con-

figuration (exactly at the top of a carbon atom). The **d** S₄-B, **e** S₄-H and **f** S₄-T configuration are shown. **g** A C₃ and **h** S₄ lateral views where the graphene–POM distances are evidenced, are also presented

Table 1 for PMo_{12} [47], $SiMo_{12}$ [36, 37] and SiW_{12} [36, 37] are in close agreement with those found with the different approaches performed in this work. As presented in Table 2, it was virtually found the same bond lengths after the clusters were relaxed in the presence of graphene, (see Fig. 2). Some slight variations were found with oscillations around 2 pm. All parameters remain virtually unaltered after geometry relaxation, evidencing the high stability of the clusters at the interaction with carbon.

The average distances Z_{C_3} and Z_{S_4} among the different XM_{12} systems and graphene are reported in Table 2. Z_{C_3} and Z_{S_4} represent the interplanar distance between the carbon substrate and a POM with C₃ and S₄ symmetries, respectively (see Fig. 2g, h, respectively). The bonding

distances range from 229 to 303 pm (found at GGA with Na-counterions), indicating that a non-covalent interaction of the electrostatic-type is formed. The results obtained from the GGA approach indicate an agreement among the charged systems and the systems where the total charge is balanced by the Na-counterions, since it was found a range of interacting planes coming from 226.8 to 285.3 pm, ranging at an equivalent interval than that found on systems with Na-counterions reported above. Consequently, these differences may be considered to be negligible. Analogous ranges are also found for the LDA approaches as shown in Table 2.

Considering that the structural parameters obtained from the GGA and LDA approaches are in close

Table 2 Interplanar distances from graphene to XMo_{12} , with $X = Pd, P, Ru, Si$ and $M = Mo, Nb, W$

	Symmetry					
	C_3 -B	C_3 -H	C_3 -T	S_4 -B	S_4 -H	S_4 -T
Interplanar distances in pm (GGA)						
System (with counterions)						
$[PdMo_{12}O_{40}]^{2-}/G$	273.0	275.3	256.5	283.7	286.2	282.0
$[PdMo_{12}O_{40}]^{6-}/G$	279.0	–	–	285.4	–	–
PMo_{12}/G	280.0	272.5	282.2	261.7	297.2	288.0
$RuNb_{12}/G$	245.1	253.8	249.4	256.2	250.0	252.3
$SiMo_{12}/G$	272.4	274.4	272.6	265.7	265.5	269.8
SiW_{12}/G	283.3	262.6	271.2	279.6	283.0	273.9
System (charged)						
$PdMo_{12}/G$	242.2	262.0	260.2	268.0	271.4	272.1
PMo_{12}/G	251.2	261.0	263.6	258.4	276.0	279.0
$RuNb_{12}/G$	239.4	260.6	236.0	246.0	242.2	253.5
$SiMo_{12}/G$	251.3	259.2	271.3	265.7	253.4	267.1
SiW_{12}/G	248.4	256.0	250.5	268.1	267.7	262.5
Interplanar distances in pm (LDA)						
System (with counterion)						
$PdMo_{12}/G$	251.6	250.3	253.0	248.3	242.9	247.3
PMo_{12}/G	252.2	281.9	264.8	259.2	297.8	289.7
$RuNb_{12}/G$	207.1	208.9	233.2	249.3	227.5	234.5
$SiMo_{12}/G$	267.6	254.4	261.1	253.6	253.4	252.8
SiW_{12}/G	261.4	259.8	255.6	260.2	266.3	275.7
System (charged)						
$PdMo_{12}/G$	243.4	252.2	247.5	253.8	258.4	254.7
PMo_{12}/G	244.9	246.4	248.6	242.0	248.8	247.3
$RuNb_{12}/G$	218.2	139.6	217.6	229.3	142.4	182.7
$SiMo_{12}/G$	219.3	235.5	233.9	237.3	242.1	233.8
SiW_{12}/G	228.6	232.1	234.7	236.7	239.9	239.6

agreement and that independently of the use of counterions or explicit charge at the POM systems during the relaxations, we can conclude that all procedures may adequately model the geometrical parameters at the POM/carbon surface interface. Furthermore, we can determine which scheme may be more optimal and computationally inexpensive. In this regard, in Fig. S1 and S2 of the Supplementary Information (SI), a computation time comparison among those calculations performed with the respective nominal charge and those with explicit counterions, is presented. For those calculations performed at GGA level (see Fig. S1), we found that in the majority of the systems, the computations performed with electronic charges is completed in shorter times than those computed with explicit counterions. In some isolated cases, this behavior is reversed but in average, the use of charges in the geometry relaxations results in faster computations. The values found in the LDA calculations (see Fig. S2) are equivalent and only the $RuNb_{12}/G$ system at the S_4 configuration results in larger computation

time than the systems with explicit counterions. Consequently, the structural properties of POM/carbon systems may be studied at the inexpensive methodology (smaller computation time) based on the use of electronic charges instead of considering the use of explicit counterions. Nevertheless, the study of more general electronic properties may only be assessed with the aid of counterions, as it is further described.

On the other hand, these preliminary results were also complemented with the computation of electronic structure properties that may be relevant in energy storage modeling, such as the adsorption energy, which was previously defined in Sect. 2. The adsorption energies computed at the GGA methodology with the charged systems and with the systems neutralized by the counterions are presented in Figs. 3 and 4, respectively. It can be seen that the interaction of the charged systems $SiMo_{12}/G$, SiW_{12}/G and PMo_{12}/G appears to be repulsive at the six different orientations where the POM systems meet the graphene surface. Such repulsion is greatest in the $RuNb_{12}/G$ system,

Fig. 3 Adsorption energies of the XM_{12} clusters adsorbed on graphene at the GGA approach (with explicit charges)

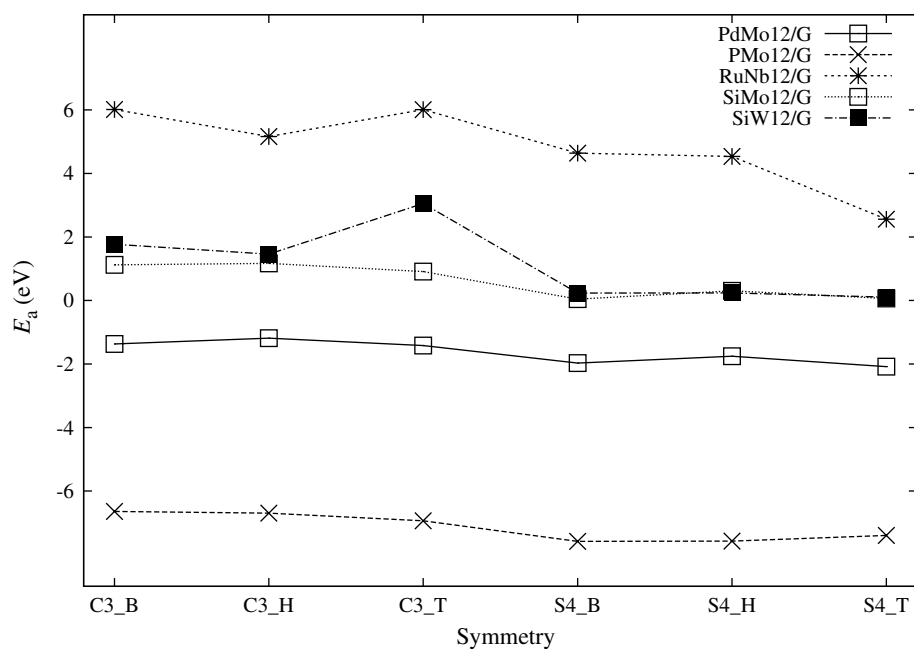
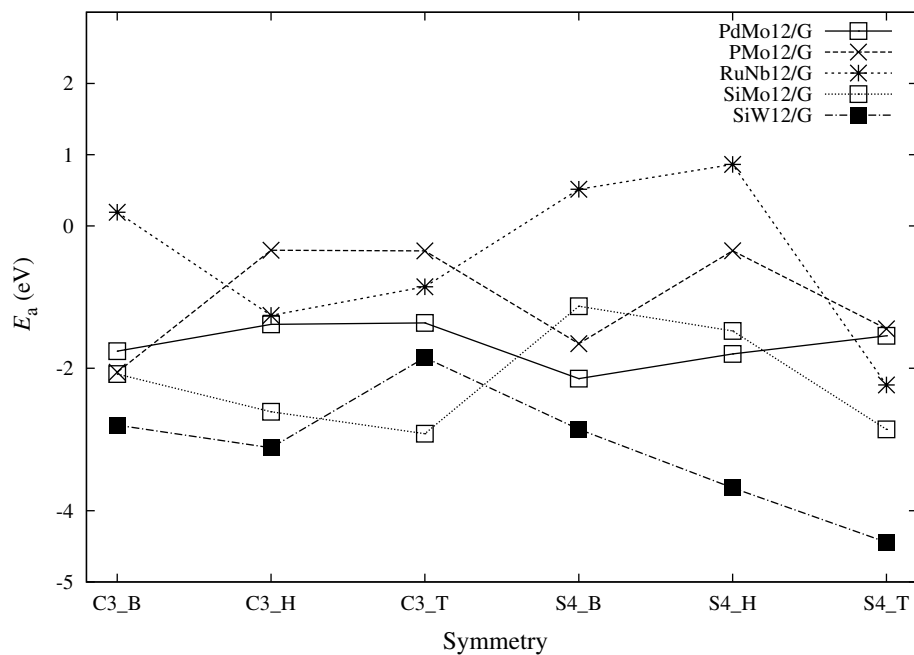


Fig. 4 Adsorption energies of the XM_{12} clusters adsorbed on graphene at the GGA approach (with Na-counterions)

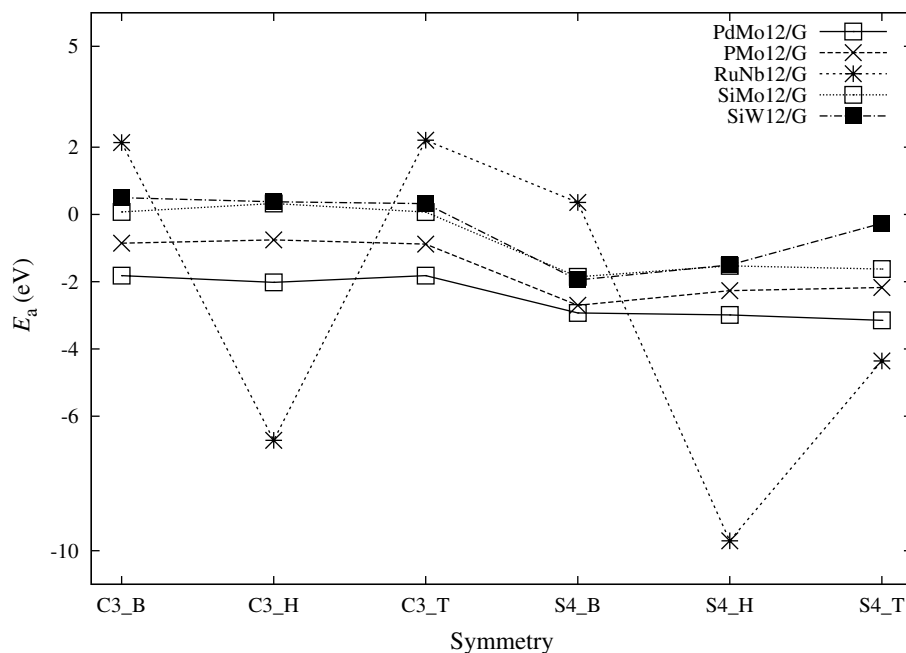


reaching a maximum at the C_3 -T orientation with a repulsion energy of about 6 eV (see Fig. 3).

An attractive energy was found for the six configurations of $PdMo_{12}/G$ and PMo_{12}/G systems. In both cases, a minimum is found at the S_4 -B symmetry with -2.0 and -7.5 eV, respectively. On the other hand, we computed the adsorption energies on the group of title systems by considering the neutralization of the respective charge on each system. As it was already outlined in the Computational details, counterions simulating point charges with values of $+1.0$ e for each unit were introduced. It was found with no

exception that all geometries present at least three different configurations where the adsorption energy is attractive. That is, the systems $SiMo_{12}/G$ (C_3 -T symmetry), SiW_{12}/G (S_4 -T symmetry) and PMo_{12}/G (S_4 -B symmetry) present an equilibrium geometry with an attractive adsorption energy, i.e., with -3.0 , -4.4 and -1.7 eV, respectively. Consequently, the SiW_{12}/G and PMo_{12}/G attractive interactions correspond to a non-covalent bonding of the electrostatic-type. Nevertheless, for the SiW_{12}/G case, the minimum energy at the S_4 -T configuration (about -4.4 eV) may be attributed to a strong attraction with a certain degree of

Fig. 5 Adsorption energies of the XM_{12} clusters adsorbed on graphene at the LDA approach (with explicit charges)



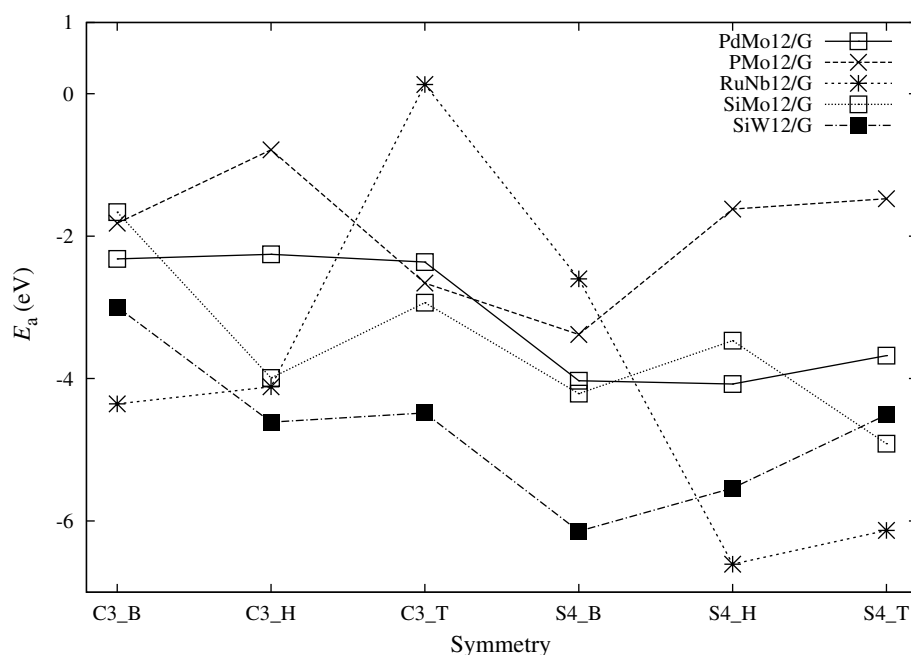
covalency. It allows the POM system to be tightly adsorbed (certainly a chemisorption may be expected) onto the graphene layer with an unprecedented attractive energy. The $\text{PdMo}_{12}/\text{G}$ system presents attractive energies in all configurations with a minimum located at the $\text{S}_4\text{-B}$ symmetry (about -2 eV), addressed also to a non-covalent interaction.

It is important to highlight that the PdMo_{12} ($[\text{PdMo}_{12}\text{O}_{40}]^{2-}$) system corresponds to Pd(VI), which may represent an uncommon state of palladium. Taking the latter into account, we performed a geometry relaxation on the $[\text{PdMo}_{12}\text{O}_{40}]^{6-}$ system. This charged species contains Pd(II), which represents a more common form of palladium. It was found that the $[\text{PdMo}_{12}\text{O}_{40}]^{6-}$ system is more stable than the $[\text{PdMo}_{12}\text{O}_{40}]^{2-}$ species and presents similar structural parameters as reported in Table 1. Note that this comparison was only performed at the GGA level in the presence of the counterions. Furthermore, we also optimized the composite system $[\text{PdMo}_{12}\text{O}_{40}]^{6-}$ adsorbed on graphene (see structural parameters at Table 2), considering the most stable geometries found for the $[\text{PdMo}_{12}\text{O}_{40}]^{2-}$ system, namely $\text{C}_3\text{-B}$ and $\text{S}_4\text{-B}$ to compare both cases. It was found that the adsorption energies for the $\text{C}_3\text{-B}$ and $\text{S}_4\text{-B}$ symmetries are $+0.397$ and $+5.681$ eV, respectively, indicating that a strong repulsion may be expected for the $[\text{PdMo}_{12}\text{O}_{40}]^{6-}$ charged species. Since $[\text{PdMo}_{12}\text{O}_{40}]^{n-}$, with $n = 2$ and 6 are both predicted species, we may conclude that $n = 6$ may be expected to be more stable at a synthesis in the experimental level, but the attraction with a carbon substrate may only be suitable with $n = 2$ charged species.

At the $\text{RuNb}_{12}/\text{G}$ system, we found three different attractive configurations of the same energetic magnitude corresponding to the non-covalent bonding found in the previous systems, i.e. $\text{C}_3\text{-H}$, $\text{S}_4\text{-B}$ and $\text{S}_4\text{-T}$ symmetries, with a minimum at the $\text{S}_4\text{-B}$ orientation (see Fig. 2). The rest of the symmetries in this system are certainly repulsive, which may be due to the high charge stored at the Keggin cage (-8.0 e). It may destabilize the frontier molecular orbitals in the system, giving as a result no physisorption in the $\text{C}_3\text{-B}$, $\text{S}_4\text{-B}$ and $\text{S}_4\text{-H}$ configurations. The latter may also be related to the bonding distances found from the graphene plane to the imaginary plane crossing the bottom of the POM cluster at the six different configurations. It was found in Table 2 that the $\text{RuNb}_{12}/\text{G}$ system presents the shortest interplanar distances in all configurations. Particularly, the RuNb_{12} cluster with $\text{C}_3\text{-B}$, $\text{S}_4\text{-B}$ and $\text{S}_4\text{-H}$ symmetries is located at 245.1, 256.2 and 250.0 pm from the graphene plane, respectively, corresponding to the closest bond distances found in the series. Such behavior may be interpreted with a certain degree of covalency that may impact POM retention onto carbon substrates, favorable for energy storage applications.

The adsorption energies computed at the LDA/CA level of theory are depicted in Fig. 5 with the charged systems and also with the presence of counterions to neutralize the overall charge (see Fig. 6). In the first case, the adsorption energies for the systems under study range from about -3.0 to 2.0 eV, such as it is reported in the charged systems at the GGA/PBE level of theory. As it was previously found, the $\text{RuNb}_{12}/\text{G}$ system presents a strong attractive adsorption energy. In this case, such interactions are certainly

Fig. 6 Adsorption energies of the XM_{12} clusters adsorbed on graphene at the LDA approach (with Na-counterions)



evidenced in the C_3 -H and S_4 -H configurations (about -6.7 and -10.0 eV, respectively).

When the calculations are performed at LDA/CA level with the presence of counterions, the range of adsorption energies is reduced and virtually all interactions among the POM systems and graphene are attractive. The covalent character found for the SiW_{12}/G at the GGA/PBE level is also reproduced at this scheme, evidencing the strongest interaction found in the series of systems under study. Using this methodology, the lowest energy corresponds to the S_4 -H configuration, and it overestimates the most stable configuration at GGA/PBE level by about -2.0 eV. Besides, the adsorption energies of the $RuNb_{12}/G$ system oscillates and the lowest adsorption energy was found at -7.0 eV. This adsorption energy may also be considered as a non-covalent attraction of the electrostatic-type. Consequently, the GGA/PBE methodology (with counterions) is to be implemented for further analysis in this work, since it smoothly reproduces the interaction energies through the series, giving no overestimations to this property, due to the improved approach provided by GGA over the local description introduced by LDA.

3.2 Charge analysis

In order to quantitatively figure out the amount of charge transfer at the relaxed geometries along the title compounds, a series of Mulliken calculations were performed by taking into account that this analysis requires to be carefully interpreted since it is highly sensitive to the basis set. For all our systems, the robust DZP basis set, as implemented in SIESTA [31–33] was used. The results are presented in

Table 3, where the GGA and LDA schemes are compared with the charged systems and those in the presence of counterions. Indeed, the $PdMo_{12}/G$ system undergoes a charge transfer that in all symmetries comes from the $PdMo_{12}$ cluster to graphene. The smallest charge transfer corresponds to the lowest energy configuration found at the GGA/PBE level in the presence of counterions, indicating that the origin of the attraction is made of a strong electrostatic attraction and it may only be mediated by an orbital behavior. Furthermore, the same tendency is also reported for the GGA/PBE level in the charged $PdMo_{12}/G$ system (see Table 3). In this regard, in order to make a comparison with the Mulliken charge analysis in the particular systems $[PdMo_{12}O_{40}]^{n-}$ (with $n = 2$ and 6) and to corroborate that no fortuitous results on the charge transfer were evaluated, we also performed a Hirshfeld charge analysis [48, 49] on both systems. Such values are reported in Table 3 (the values given in parenthesis), and it was found that for the $[PdMo_{12}O_{40}]^{2-}$ system, a charge of about $+0.160$ e was depleted from the POM, for the C_3 -B and S_4 -B symmetries. The charge was transferred to the carbon substrate. A similar behavior was also observed with the Mulliken charge analysis. Furthermore, the Hirshfeld charge analysis performed in the system $[PdMo_{12}O_{40}]^{6-}$ adsorbed on graphene, indicates that about $+3.00$ e were transferred from the POM to the carbon sheet, despite the repulsion found in this particular configuration. This behavior was also found by using the Mulliken charge analysis, as it is reported in Table 3. Both schemes, Hirshfeld and Mulliken analyses, reveal the imminent charge transfer from the POM to the carbon substrate. On the other hand, the system PMo_{12}/G presents a minimum located at the S_4 -B symmetry (charged and with counterions) when it is optimized with the GGA/PBE

Table 3 Charge transfer using Mulliken analysis from XMo_{12} to graphene, with X = Pd, P, Ru, Si and M = Mo, Nb, W

	ΔQ (e)						
	<i>n</i>	C ₃ -B	C ₃ -H	C ₃ -T	S ₄ -B	S ₄ -H	S ₄ -T
ΔQ (GGA)							
System (with counterions)							
PdMo ₁₂ /G	-2	+0.128 (0.155)	+0.122	+0.115	+0.082 (0.154)	+0.093	+0.092
PdMo ₁₂ /G	-6	+3.287 (3.308)	-	-	+2.986 (3.055)	-	-
PMo ₁₂ /G	-3	+1.112	+1.157	+1.167	+1.083	+1.175	+1.093
RuNb ₁₂ /G	-8	+3.554	+3.561	+3.581	+3.299	+3.281	+3.308
SiMo ₁₂ /G	-4	+1.932	+1.886	+1.966	+1.811	+1.765	+1.831
SiW ₁₂ /G	-4	+2.194	+2.182	+2.140	+2.226	+2.287	+2.091
System (charged)							
PdMo ₁₂ /G	-2	+0.087	+0.087	+0.427	+0.017	+0.026	+0.030
PMo ₁₂ /G	-3	+0.463	+0.453	+0.420	+0.229	+0.239	+0.256
RuNb ₁₂ /G	-8	+3.066	+3.144	+3.069	+2.716	+3.312	+2.888
SiMo ₁₂ /G	-4	+0.940	+0.951	+1.050	+0.712	+1.659	+0.722
SiW ₁₂ /G	-4	+0.956	+0.954	+0.953	+0.782	+0.789	+0.786
ΔQ (LDA)							
System (with counterion)							
PdMo ₁₂ /G	-2	+0.204	+0.240	+0.241	+0.204	+0.211	+0.216
PMo ₁₂ /G	-3	+1.128	+1.208	+1.157	+1.094	+1.185	+1.108
RuNb ₁₂ /G	-8	+3.909	+3.866	+3.677	+3.402	+3.387	+3.395
SiMo ₁₂ /G	-4	+2.004	+1.944	+1.988	+1.840	+1.838	+1.187
SiW ₁₂ /G	-4	+2.517	+2.293	+2.240	+2.384	+2.422	+2.273
System (charged)							
PdMo ₁₂ /G	-2	+0.033	+0.029	+0.043	-0.142	-0.144	-0.041
PMo ₁₂ /G	-3	+0.653	+0.625	+0.600	+0.428	+0.438	+0.499
RuNb ₁₂ /G	-8	+3.397	+3.388	+3.198	+2.806	+2.955	+2.813
SiMo ₁₂ /G	-4	+1.317	+1.303	+0.955	+1.175	+1.171	+1.162
SiW ₁₂ /G	-4	+0.956	+0.954	+0.953	+0.782	+0.789	+0.786

methodology. This is in agreement with the results found by Muñiz et al. [30].

Charge transfer in this case (see Table 3) appears to be the smallest of the group, revealing an analogous bonding than that presented before (electrostatic with certain contribution coming from the orbital transfer). As it is depicted in Fig. 3, the behavior of the charged PMo₁₂/G system is quite plane, showing no clear minima, despite the variations on the bonding distances of equilibrium among the POM systems and graphene. Nevertheless, the charge transfer obtained with this methodology is consistent with the counterions scheme at the same level of theory.

The lowest adsorption energy found at the LDA/CA (with counterions) does not correspond to that found at the GGA/PBE level. The same tendency in the charge transfer is found, revealing that the smallest transfer is produced in the S₄-B configurations. Nevertheless, the LDA/CA Mulliken analysis for the PdMo₁₂/G system at the charge configuration returns negative values (see Table 3), addressing a transfer from graphene to the POM and indicating that

at this level of theory, the Mulliken analysis may lead to unphysical results.

Taking into consideration that in the RuNb₁₂/G system, the adsorption energy is underestimated when it is calculated with the charged system at the GGA/PBE methodology and it is overestimated at the LDA/CA method. Mulliken analysis was only considered in the schemes where the counterions were explicitly specified. Furthermore, an analogous tendency is also observed in the LDA/CA case, where the smallest adsorption energy is also overestimated (see Fig. 6). Consequently, the only Mulliken analysis that would provide physical insights is that reported by the GGA/PBE method. The charge transfer in this case (see Table 3) is the largest in the series of complexes due to the high electronic charge that the RuNb₁₂ system may retain (-8.0 e). The smallest charge transfer is reported for the S₄ symmetries and consistent with the lowest adsorption energy reported at the S₄-T symmetry.

As already found for the RuNb₁₂ cluster, the SiMo₁₂ and SiW₁₂ systems may also retain high electronic charges

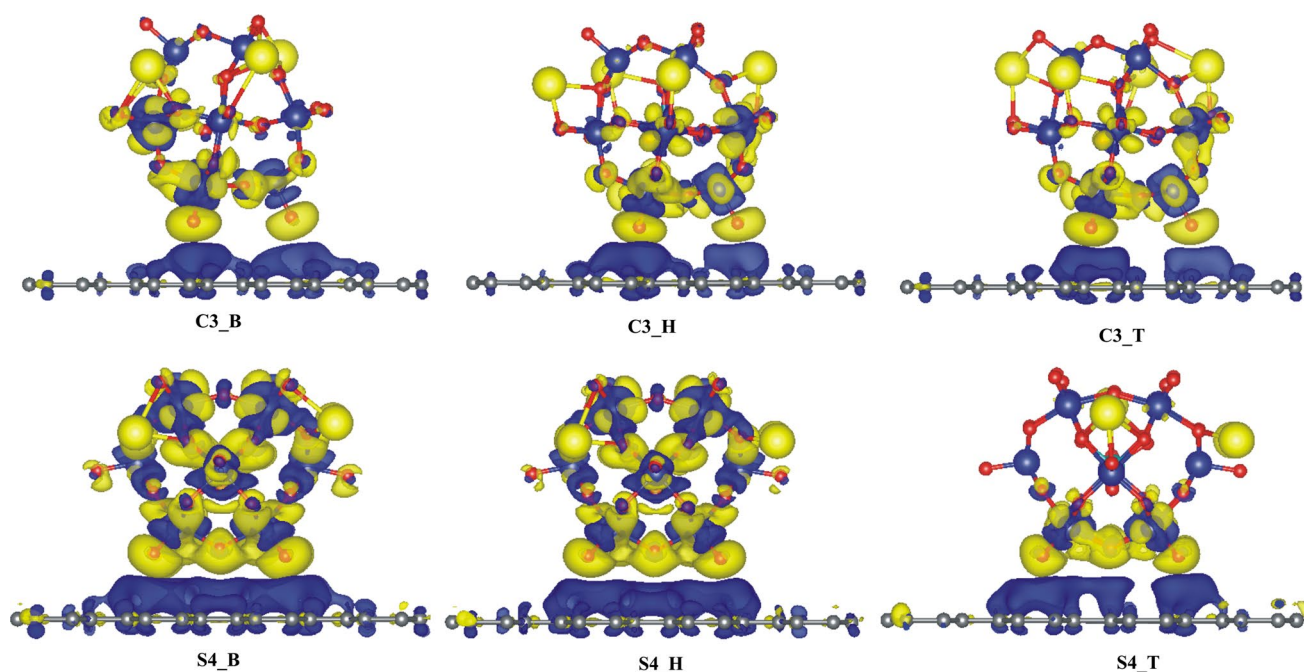


Fig. 7 Isosurfaces of density difference [$\rho_{\text{diff}}(r)$] for the system SiW_{12}/G . The six different configurations are depicted. The *blue* regions represent zones where the electronic charge has been trans-

ferred to, while the *yellow* region represent zones where charge has been depleted. All isovalues were presented with $0.002 e/(\text{a.u.})^3$

($-4.0 e$ for both cases). The interaction between both systems is essentially repulsive when it is modeled at GGA or LDA (charged systems). The tendency is reversed after introducing explicit counterions in the calculations for both methodologies. Particularly at GGA/PBE, it was found that one of the smallest charge transfers coming from the SiMo_{12} to graphene, corresponds to the $\text{S}_4\text{-T}$ symmetry, which is one of the lowest energy configurations. Furthermore, one of the smallest charge transfer found for the SiW_{12} cluster is that of the $\text{S}_4\text{-H}$ symmetry, which is also one of the lowest adsorption energies in the group.

3.3 Density difference analysis [$\rho_{\text{diff}}(r)$]

Charge transfer was also studied from the electronic density difference [$\rho_{\text{diff}}(r)$] isosurfaces, as defined in Sect. 2. The $\rho_{\text{diff}}(r)$ isosurfaces are shown in Figs. 7 and 8 for the lowest-adsorption energy systems. Such systems correspond to SiW_{12}/G and $\text{SiMo}_{12}/\text{G}$, showing the lowest-adsorption energies through all possible geometrical configurations along the series, according to the calculations performed at GGA and explicit Na-counterions. The blue color in both figures represents zones where electronic charge has been transferred to, while the yellow color represents those zones where charge has been depleted. We virtually found in all series that the electronic charge is transferred to the region between the bottom of the cluster and just above the graphene plane. These results are in close agreement with

the quantitative predictions obtained with the Mulliken analysis. Furthermore, this is consistent with the experimental evidence obtained by Wang et al. [5], since it was found that in the analogous $\text{H}_4\text{SiW}_{12}\text{O}_{40}/\text{G}$ nanohybrid system, the SiW_{12} transfers the electrons from the electrode to the graphene oxide, where the content of oxygen-containing groups is decreased to about 5%. The isosurfaces of all systems in the series are also reported, obtained at GGA and LDA approaches considering the presence of n -Na counterions, where $n = 2, 3, 4$ and 8 , depending on the POM under study (see Table 3 for reference). Those isosurfaces are presented from Figures S3 to S10 at the Supplementary Information (SI). Independently of the chosen method, we found that the charge is always transferred to the adjacent regions of the POM cluster.

3.4 Density of states (DOS)

Considering that the most reliable methodology in our series of computations was found to be the GGA/PBE level of theory with the presence of explicit counterions, the analysis within this scheme to the study of the electronic density of states was extended. We studied the first two systems with lowest adsorption energies. That is, for the system $\text{PdMo}_{12}/\text{G}$, these geometries are the $\text{C}_3\text{-B}$ and $\text{S}_4\text{-B}$ symmetries. Figure 9 shows the total DOS (continuous blue line), revealing that the well-known non-semiconducting character of graphene is altered due to the rising of states

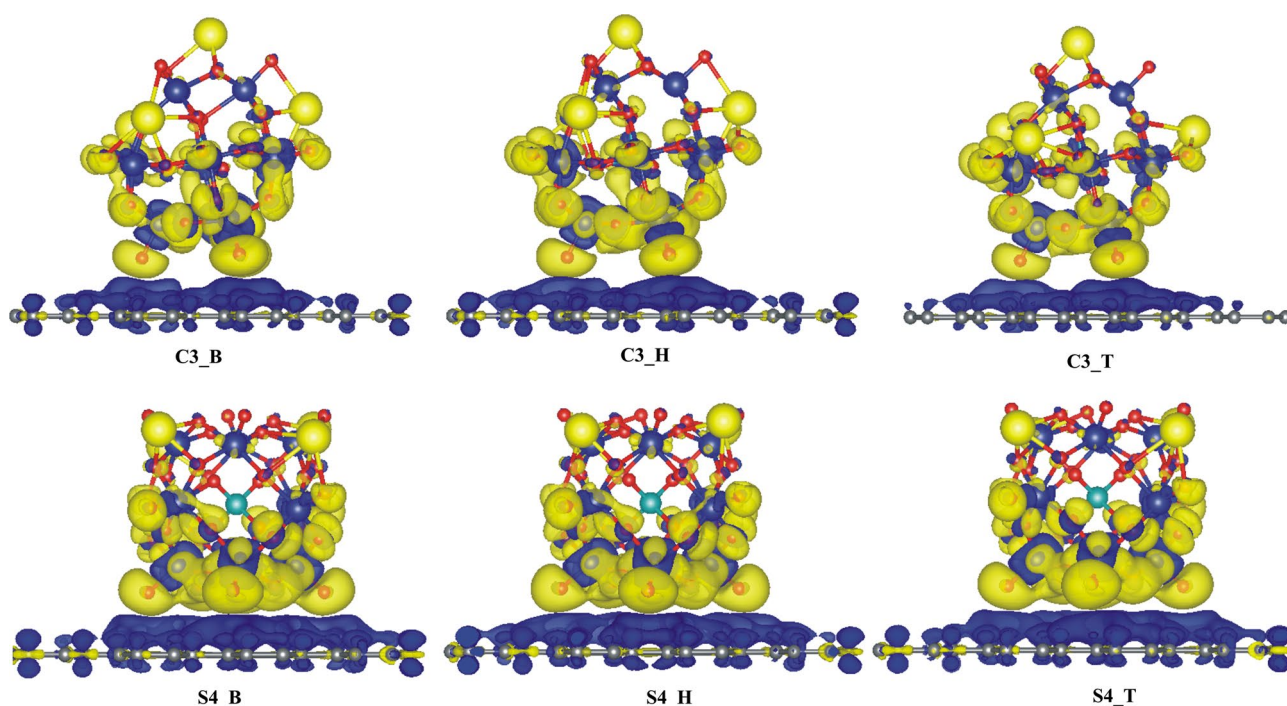


Fig. 8 Isosurfaces of density difference $[\rho_{\text{diff}}(r)]$ for the system $\text{SiMo}_{12}/\text{G}$. The six different configurations are depicted. The *blue regions* represent zones where the electronic charge has been trans-

ferred to, while the *yellow region* represent zones where charge has been depleted. All isovalues were presented with $0.002 e/(\text{a.u.})^3$

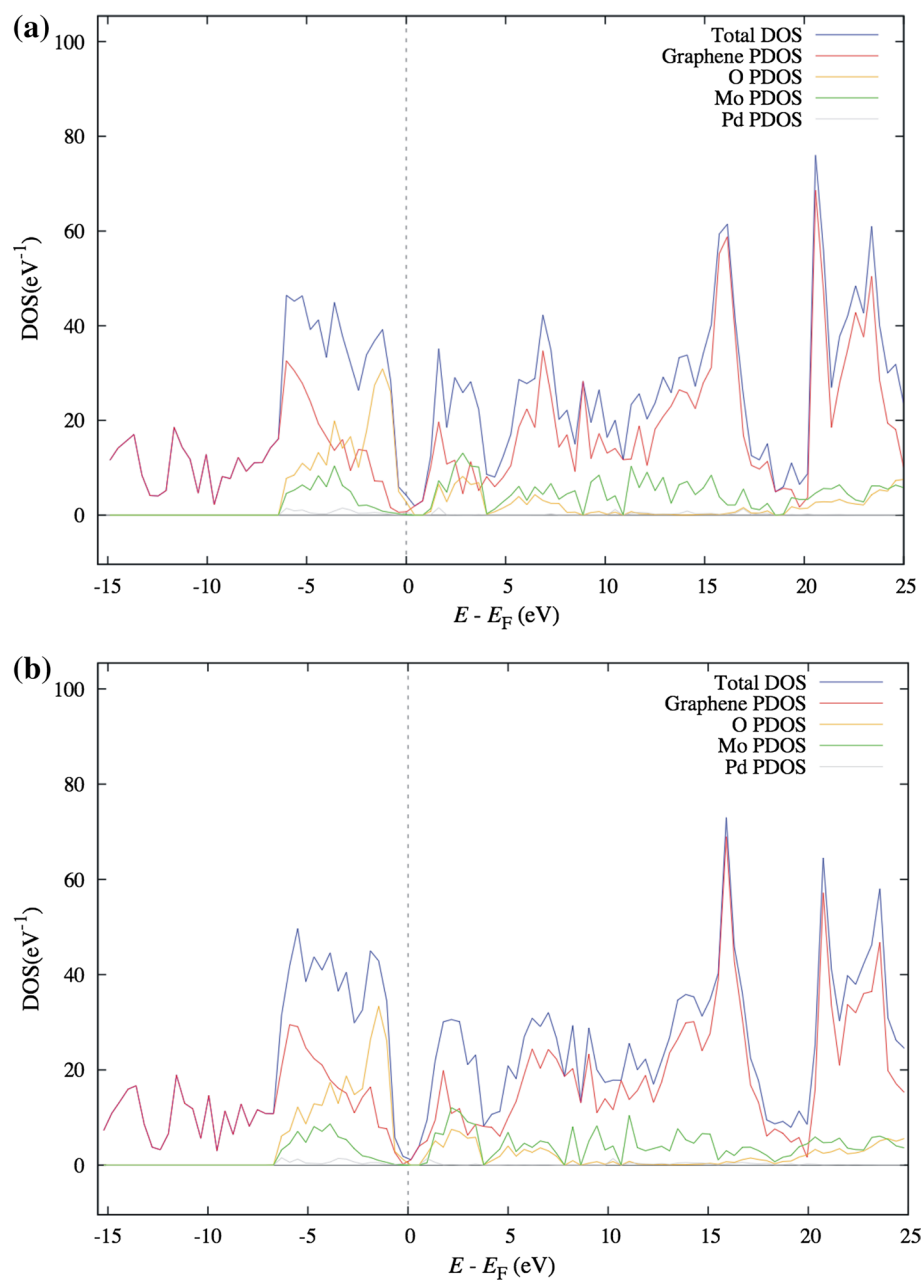
around the Fermi level, as it can be clearly seen in the $\text{C}_3\text{-B}$ case.

The rising of these unprecedented states may be addressed to new pathways that ions may follow in the charge/discharge process of a battery or supercapacitor, that allows the electronic charge to be retained more effectively than those cases where no metallic clusters is present on the supercapacitor electrode and only a carbon nanostructure rules the charge retention. An analogous behavior is also reported for the PMo_{12}/G system (as depicted in Fig. S11 of SI), where the $\text{C}_3\text{-T}$ and $\text{S}_4\text{-B}$ symmetries represent the lowest adsorption energies. In both cases, the projected density of states (PDOS) of carbon reveals the characteristic V-shape of the non-semiconducting nature of graphene [30], which is significantly distorted due to the contributions coming from the PDOS of oxygen atoms, but more importantly from the PDOS of Mo atoms that radically enhance the DOS around the Fermi level, giving the nanohybrid structure a 'metallic-like' character, as it was previously reported by Muñiz et al. [30]. It is important to highlight that the contributions coming from the P central atom are virtually negligible, since the P atom is located far from the interlayer region, where the POM interacts with the carbon layer. The Na^+ counterions give no contributions to the total DOS since their formal charge in the

system is +1 and no electronic states are expected. The total DOS and PDOS of the high charged systems ($-8.0 e$) $\text{RuNb}_{12}/\text{G}$ were computed for the $\text{C}_3\text{-H}$ and $\text{S}_4\text{-T}$ symmetries, as depicted in Fig. 10. In this nanohybrid structure, the mechanism is quite different and the non-semiconducting nature of graphene is preserved, but slightly shifted below the Fermi level in the $\text{S}_4\text{-T}$ symmetry, probably due to the destabilization provoked by the large total charge. Contrary to the $\text{PdMo}_{12}/\text{G}$ and PMo_{12}/G systems, the DOS coming from the oxygen atoms have a large contribution that significantly enhances the total DOS. The PDOS from the peripheral Nb atoms have only small contributions to the total DOS, and finally the total DOS is certainly strengthened as depicted in Fig. 10. This novel and modified DOS of both nanostructures may represent an excellent candidate in a hybrid supercapacitor electrode, since it is highly likely that the charge would be retained much more effectively than in systems such as PMo_{12}/G [8, 30]. The Nb PDOS moderately contribute to the total DOS at the Fermi level, but are responsible for the DOS contributions above the Fermi level.

The system $\text{SiMo}_{12}/\text{G}$ charged with $-4.0 e$ also reveals a shifting below the Fermi level for the carbon PDOS (see Fig. 11), which may also be attributed to the destabilization in the electronic structure of the POM, due to the high

Fig. 9 Total density of states (DOS) and projected density of states (PDOS) in a.u. of system PdMo₁₂/G. The dashed line indicates the location of the Fermi energy. **a** C₃-B and **b** S₄-B configurations, respectively (lowest energy symmetries of this series)

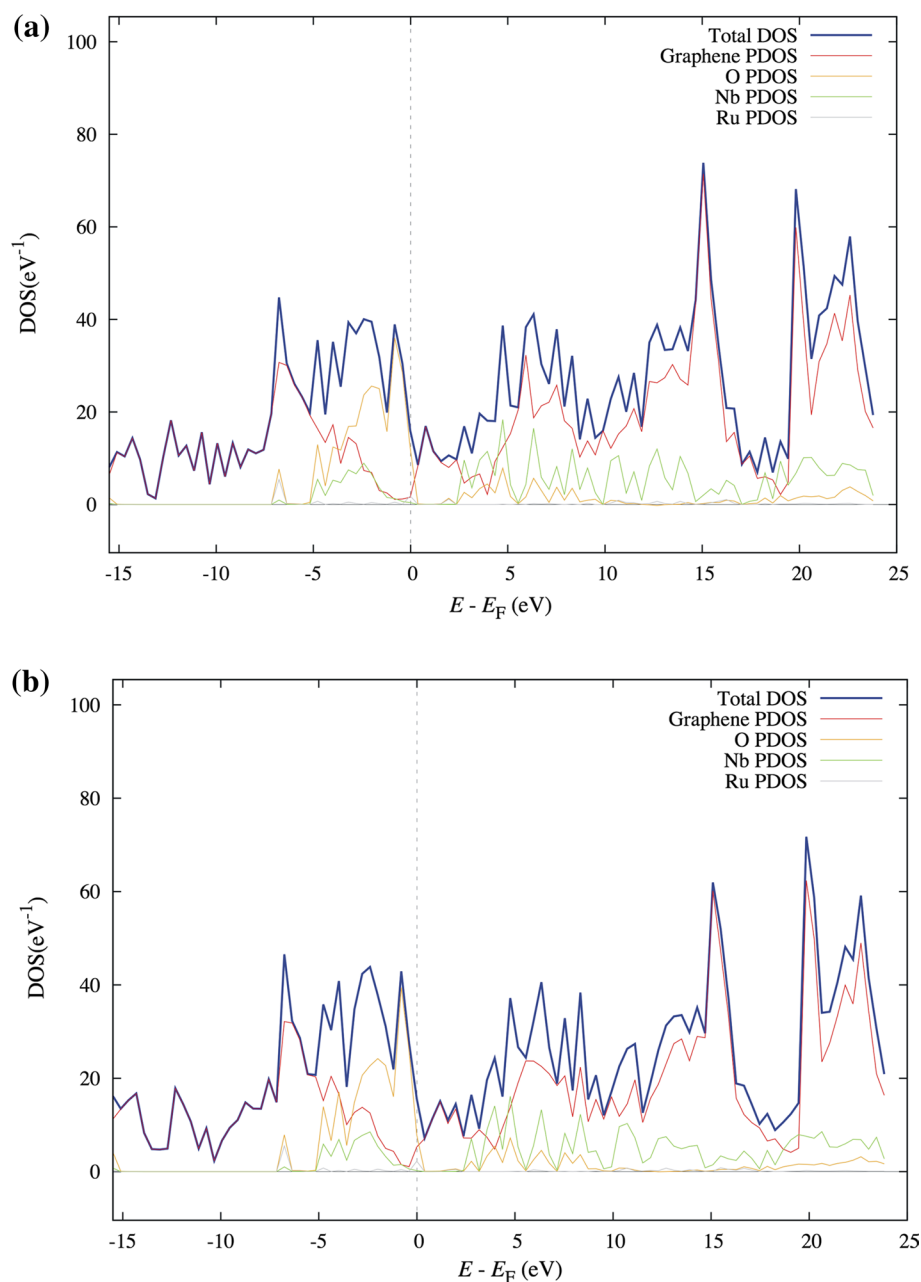


electronic charge supported by the POM. The presence of the Mo–O bonding in the POM presents the same behavior than that reported in PdMo₁₂/G and PMo₁₂/G systems. The PDOS contributions coming from Mo atoms enhances the metallic character of the nanohybrid around the Fermi level. This trend was also found in the SiW₁₂/G system (as presented in Fig. S12 of SI), but in this case the W PDOS take the role of the Mo PDOS, and significantly enhances the total DOS around the Fermi level. Consequently, SiMo₁₂ and SiW₁₂ may also play a role as metallic oxides deposited on graphene, which would be capable to achieve electronic charge retention more effectively.

4 Conclusions

A systematic study on the electronic structure properties of a series of Keggin clusters XM₁₂ supported on a carbon substrate was performed for the first time. GGA and LDA approaches were used by considering the presence of the nominal charges of the clusters and also by introducing Na-counterions to neutralize the overall charge. The structural parameters lie at the same range in both methodologies, which evidences that both approaches may be implemented to characterize the systems. Further, we can decide to use the most inexpensive method to model

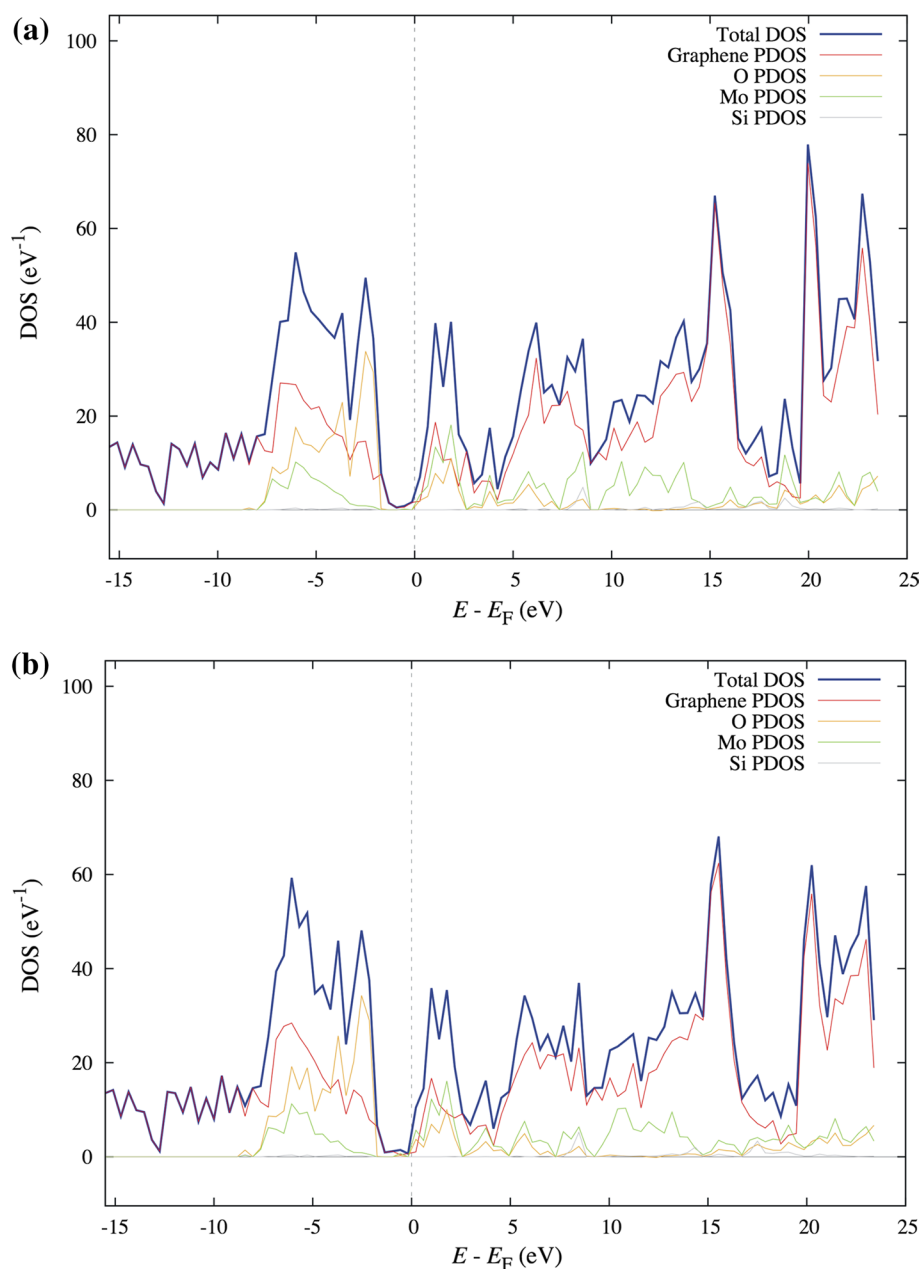
Fig. 10 Total density of states (DOS) and projected density of states (PDOS) in a.u. of system RuNb₁₂/G. The *dashed line* indicates the location of the Fermi energy. **a** C₃-H and **b** S₄-T configurations, respectively (lowest energy symmetries of this series)



a POM/carbon interaction. Nevertheless, only the adsorption energies computed at the GGA level (with Na-counterions) may give us physical insights into the origin of the bonding between the series of POMs and the graphene substrates, since charge neutralization plays an important role to stabilize the hybrid system. The results indicate that a non-covalent bonding of the electrostatic-type is the mechanism behind the attraction in both materials. From a Mulliken analysis, a charge transfer was found from the metallic cluster to carbon, which is also evidenced in the

isosurfaces of electronic density differences. The re-ordering in charge density was also analyzed with the DOS and PDOS, revealing the strengthening of electronic states around the Fermi level, which would facilitate the ion transport in energy storage devices. Particularly, promising candidates that fulfill this requirement are the RuNb₁₂/G, SiW₁₂/G and SiMo₁₂/G cases. The strong adsorption energies and enhanced DOS around the Fermi level evidence it. These systems are potential candidates that for instance may enhance the energy storage properties observed

Fig. 11 Total density of states (DOS) and projected density of states (PDOS) in a.u. of system SiMo_2/G . The *dashed line* indicates the location of the Fermi energy. **a** $\text{C}_3\text{-T}$ and **b** $\text{S}_4\text{-T}$ configurations, respectively (lowest energy symmetries of this series)



experimentally. The methodology developed in this work may aid in the discovery of novel materials that may be reliable for high performance energy storage devices.

Acknowledgements The authors want to acknowledge the support given by Cátedras-CONACYT (Consejo Nacional de Ciencia y Tecnología) under Project No. 1191, DGTIC (Dirección General de Cómputo y de Tecnologías de Información y Comunicación) and the Supercomputing Department of Universidad Nacional Autónoma de México for the computing resources under Project No. SC16-1-IR-29. C.C. wants to acknowledge the financial support given by CONACYT with the Ph.D. Scholarship No. 539402. A.M.O. would like to acknowledge the financial support given by Consejo de Ciencia y Tecnología del Estado de Chiapas (COCYTECH) under Project No. 14318. The authors also acknowledge the National Supercomputer Center (CNS) of IPICYT, A.C. for supercomputer facilities, and those

are: Thubat-Kaal. The authors would like to acknowledge the financial support given by DGAPA (Dirección General de Asuntos del Personal Académico) under Project No. IN112414. We also thank LCC Tiare Robles Bonilla for technical assistance in the development of Python scripts for data management.

References

1. Franco AA, Liesse ML, Bessler WG (2016) Physical multiscale modeling and numerical simulation of electrochemical devices for energy conversion and storage. Springer, Berlin
2. Qiu Y, Chen Y (2015) J Phys Chem C 119:23813
3. Genovese M, Lian K (2015) Curr Opin Solid State Mater Sci 19:126

4. Ji Y, Huang L, Hu J, Streb C, Song YF (2015) *Energy Environ Sci* 8:776
5. Wang S, Li H, Li S, Liu F, Wu D, Feng X, Wu L (2013) *Chem Eur J* 19:10895
6. Suárez-Guevara J, Ruiz V, Gómez-Romero P (2014) *PCCP* 16:20411
7. Tessonnier J, Goubert-Renaudin S, Alia S, Yan Y, Barteau M (2013) *Langmuir* 29:393
8. Cuentas-Gallegos A, López-Cortina S, Brousse T, Pacheco-Catalán D, Fuentes-Quezada E, Mosqueda H, Orozco-Gamboa G (2016) *J Solid State Electrochem* 20:67
9. Long DL, Tsunashima R, Cronin L (2010) *Angew Chem Int Ed* 49:1736
10. Wang X, Wang E, Lan Y, Hu C (2002) *Electroanalysis* 14:1116
11. Liu H, He P, Li Z, Sun C, Shi L, Liu Y, Zhu G, Li J (2005) *Electrochem Commun* 7:1357
12. Koper M (2013) *Nat Chem* 5:255
13. Bianchini C, Shen P (2009) *Chem Rev* 109:4183
14. Xu J, Cao X, Xia J, Gong S, Wang Z, Lu L (2016) *Anal Chim Acta*. doi:10.1016/j.aca.2016.06.033 (in press)
15. Kawasaki N, Wang H, Nakanishi R, Hamanaka S, Kitaura R, Shinohara H, Yokoyama T, Yoshikawa H, Awaga K (2011) *Angew Chem Int Ed* 50:3471
16. Azumi B, Ishihara T, Nishiguchi H, Takita Y (2002) *Electrochemistry* 70:869
17. Cuentas-Gallegos A, González-Toledo M, Rincón M (2007) *Rev Mex Fis S* 53:91
18. Cuentas-Gallegos A, Martínez-Rosales R, Baibarac M, Gómez-Romero P, Rincón ME (2007) *Electrochem Commun* 9:2088
19. Baeza-Rostro D, Cuentas-Gallegos A (2013) *J New Mater Electrochem Syst* 13:203
20. Cuentas-Gallegos A, Jiménez-Penalzoa S, Baeza-Rostro D, German-García A (2010) *J New Mater Electrochem Syst* 13:369
21. Ruiz V, Suárez-Guevara J, Gómez-Romero P (2012) *Electrochem Commun* 24:35
22. Suárez-Guevara J, Ruiz V, Gómez-Romero P (2014) *J Mater Chem A* 2:1014
23. Garrigue P, Delville M, Labrugere C, Cloutet E, Kulesza P, Morand J, Kuhn A (2004) *Chem Mater* 16:2984
24. Li H, Pang S, Wu S, Feng X, Mullen K, Bubeck C (2011) *J Am Chem Soc* 133:9423
25. Xu D, Chen WL, Li JS, Sang XJ, Lu Y, Su ZM, Wang EB (2015) *J Mater Chem* 3:10174
26. Wen S, Guan W, Kan Y, Yang G, Ma N, Yan L, Su Z, Chen G (2013) *Phys Chem Chem Phys* 15:9177
27. Yang M, Gill-Choi B, Chul-Jung YKHS, Suk-Huh Y, Bok-Lee S (2014) *Adv Funct Mater* 24:7301
28. Rozanska X, Sautet P, Delbecq F, Lefebvre F, Borshch S, Chermette H, Basset JM, Grinenval E (2011) *Phys Chem Chem Phys* 13:15955
29. Aparicio-Angles X, Miro P, Clotet A, Bo C, Poblet JM (2012) *Chem Sci* 3:2020
30. Muñoz J, Cuentas-Gallegos AK, Robles M, Valdez M (2016) *Theor Chem Acc* 135:92
31. Ordejón P, Artacho E, Soler J (1996) *Phys Rev B Condens Matter Mater Phys* 53:R10441
32. Sánchez-Portal D, Ordejón P, Artacho E, Soler JM (1997) *Int J Quantum Chem* 65:453
33. Soler JM, Artacho E, Gale JD, García A, Junquera J, Ordejón P, Sánchez-Portal D (2002) *J Phys Condens Matter* 14:2745
34. Miras HN, Yan J, Long DL, Cronin L (2012) *Chem Soc Rev* 41:7403
35. Lopez X, Carbo J, Bo C, Poblet JM (2012) *Chem Soc Rev* 41:7537
36. Gao S, Cao R, Bi W, Li X, Lin Z (2005) *Microporous Mesoporous Mater* 80:139
37. Meng JX, Wang XL, Wang EB (2009) *Transit Metal Chem* 34:361
38. Kostyrko T, Lambert CJ, Bulka BR (2010) *Phys Rev B Condens Matter Mater Phys* 81:085308
39. Wen SZ, Yang GC, Yan LK, Lii HB, Su ZM (2012) *ChemPhysChem* 14:610
40. Monkhorst H, Pack J (1976) *Phys Rev B* 13:5188
41. Blum V, Gehrke R, Hanke F, Havu P, Havu V, Ren X, Reuter K, Scheffler M (2009) *Comput Phys Commun* 180:2175
42. Mulliken R (1955) *J Chem Phys* 23:1833
43. Arellano J, Molina L, Rubio A, Alonso J (2000) *J Chem Phys* 112:8114
44. Momma K, Izumi F (2011) *J Appl Crystallogr* 44:1272
45. Merlet C, Rotenberg B, Madden PA, Taberna PL, Simon P, Gogotsi Y, Salanne M (2012) *Nat Mater* 11:306
46. Mejía-Mendoza LM, Valdéz-González M, Muñoz J, Santiago U, Cuentas-Gallegos AK, Robles M (2016) (to be published)
47. Liu S, Wang C, Zhai H, Li D (2003) *J Mol Struct* 654:215
48. Hirshfeld FL (1977) *Theor Chem Acta* 44:129
49. Fonseca-Guerra C, Handgraaf JW, Baerends EJ, Bickelhaupt FM (2003) *J Comput Chem* 25:189